Pergamon

Journal of Structural Geology, Vol. 16, No. 8, pp. 1139 to 1157, 1994

0191-8141/94 $07.00+0.00

0191-8141(93)E0001-2

TEM and AEM constraints on the origin and significance of chlorite–mica stacks in slates: an example from Central Wales, U.K.*

GEJING LI and DONALD R. PEACOR

Department of Geological Sciences, University of Michigan, Ann Arbor, MI 48109-1063, U.S.A.

R. J. MERRIMAN

British Geological Survey, Keyworth, Nottingham NG12 5GG, U.K.

B. ROBERTS

Geology Department, Birkbeck College, Malet Street, London WC1E 7HX, U.K.

and

BEN A. VAN DER PLUIJM

Department of Geological Sciences, University of Michigan, Ann Arbor, MI 48109-1063, U.S.A.

(*Received* 30 *September* 1992; *accepted in revised form* 18 *October* 1993)

Abstract—Chlorite–mica stacks (grains of intergrown chlorite and white mica) in a matrix of fine-grained white mica and chlorite have been studied using XRD, SEM, EMPA, TEM and AEM methods. The stacks occur in a weakly cleaved Llandoverian mudstone, central Wales, which has a white mica (illite) crystallinity index of 0.35° $\Delta 2\theta$ corresponding to the lower anchizone. White mica occurs as packets (100 Å to 8 μm thick) interleaved with dominant chlorite packets in stacks, with both apparent coherent interfaces or cross-cutting small angle boundaries with chlorite layers. It is well-crystallized $2M_1$ polytype with phengitic composition and low paragonite component [Na/(Na+K) ≤ 0–0.07]. Chlorite in stacks is Fe-rich and relatively homogeneous. TiO_2 crystals surround stacks and occur within chlorite, and white mica is Ti-rich compared to matrix white mica.

Fine-grained white mica and chlorite in the matrix have two different orientations: one parallel to bedding and one parallel to cleavage, which is approximately 30–50° to bedding. Matrix white mica is predominantly a $2M_1$ polytype, but some cleavage-parallel white mica is $3T$ and some bedding-parallel white mica is $1M_d$. It is Na-rich [Na/(Na+K) ~ 0.14–0.42] and relatively heterogeneous; some discrete paragonite and phengitic muscovite are observed to coexist in the cleavage orientation. Matrix white mica and chlorite each contain less Fe than corresponding white mica and chlorite in stacks. Both matrix and stack chlorite are one-layer polytypes.

The data imply that chlorite in the stacks is largely derived from the replacement of volcanogenic biotite and other ferromagnesian minerals (probably via intermediate expandable trioctahedral phyllosilicates). Most intergrowths of chlorite and mica in stacks formed by mica replacement of chlorite and altered biotite along cleavage fissures. Subsequent deformation caused further modification of pre-existing chlorite–mica stacks whereas partial dissolution of stacks and bedding-parallel matrix phyllosilicates resulted in the formation of cleavage-parallel phyllosilicates.

INTRODUCTION

COARSE phyllosilicate grains, each consisting of a stack of packets of mica and chlorite are common in Lower Paleozoic mudstones that have undergone diagenesis and low-grade regional metamorphism in the Welsh Basin (Attlewell & Taylor 1969, Brenchley 1969, Evans & Adams 1975, Fitches & Johnson 1978, Craig *et al.* 1982, Woodland 1982, 1985, Dimberline 1986, Milodowski & Zalasiewicz 1991, Li *et al.* 1992). They usually consist of intergrowths of chlorite and white mica that are generally stacked parallel or subparallel to (001) planes, and are up to 150 μm in longest dimension. Such chlorite–mica stacks have been reported from many other localities in both low-grade metamorphosed (Hoeppener 1956, Voll 1960, Kossovskaya & Shutov 1970, Williams 1972, Holeywell & Tullis 1975, Bayly *et al.* 1977, Beutner 1978, Roy 1978, White & Knipe 1978, Weber 1981, Morad 1986) and unmetamorphosed mudrocks (Pye & Krinsley 1983), although different terms have been used to describe them (see review by van der Pluijm & Kaars-Sijpesteijn 1984).

Various origins have been suggested for the formation of the chlorite–mica stacks, including: (1) strain-controlled growth and dissolution of chlorite in deformed detrital micas (Voll 1960, van der Pluijm & Kaars-Sijpesteijn 1984); (2) strain-controlled 'porphyroblasts' formed during metamorphism (Attlewell & Taylor 1969, Weber 1981); (3) pre-sedimentation, detrital

*Contribution No. 494 from the Mineralogical Laboratory, Department of Geological Sciences, University of Michigan, Ann Arbor, MI 48109-1063, U.S.A.

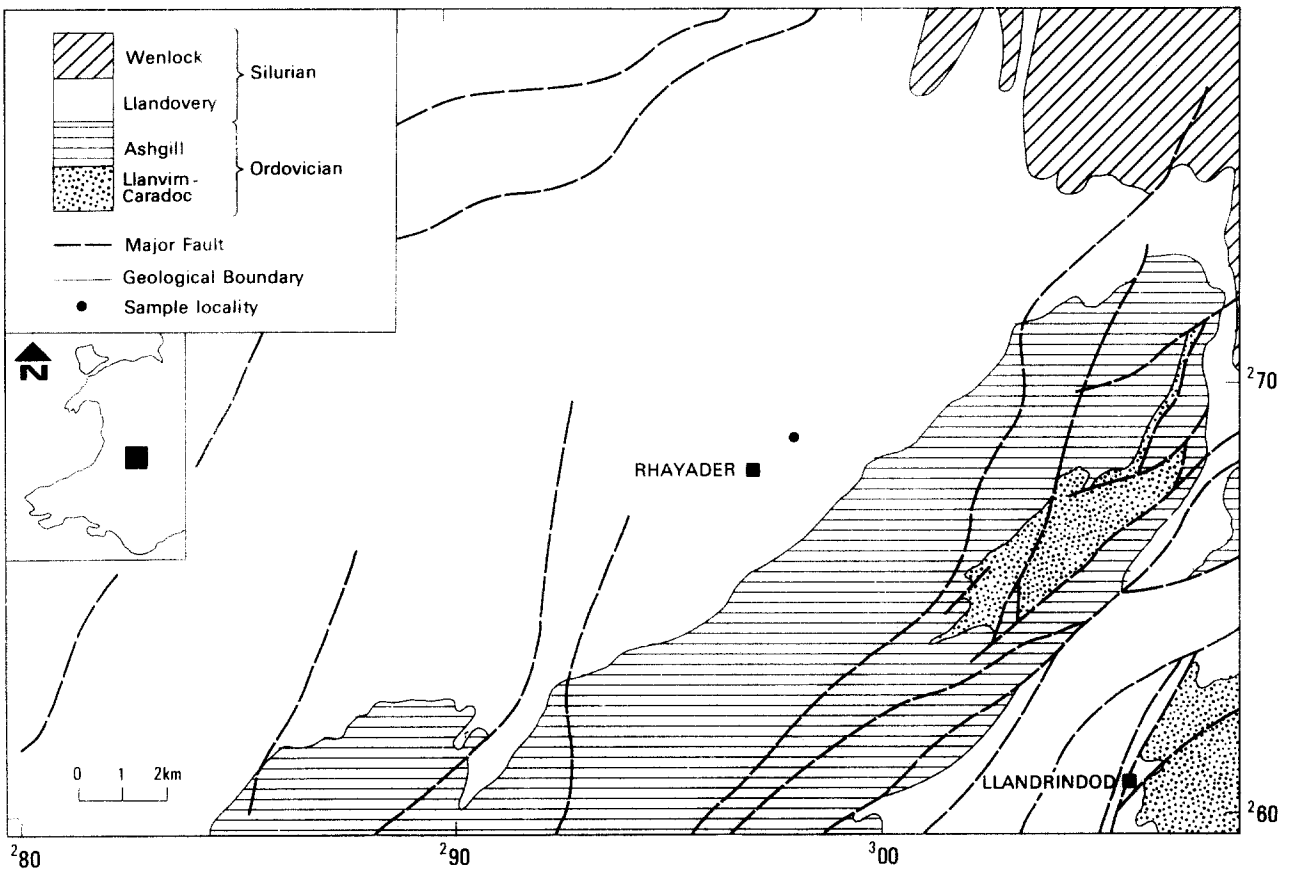

Fig. 1. Geological sketch map (after British Geological Survey 1992) showing location of sample studied.

origin (Beutner 1978); (4) pre-tectonic mimetic replacement of clay minerals (smectite) by chlorite and illite during diagenesis and low-grade metamorphism (Craig *et al.* 1982, Woodland 1982, 1985); and (5) alteration of detrital biotite to chlorite and illite during diagenesis and low-grade metamorphism (White *et al.* 1985, Dimberline 1986, Morad 1986, Milodowski & Zalasiewicz 1991).

Chlorite–mica stacks have been intensively studied by many workers. The various research methods used to characterize chlorite–mica stacks, including optical microscopy, X-ray diffraction (XRD), scanning electron microscopy (SEM) and electron microprobe analysis (EMPA), however, do not provide detailed resolution of intergrown phases in the stacks nor of the enclosing fine-grained matrix phyllosilicates. The latter also consist of mica and chlorite and are thus relevant to the paragenetic evolution of chlorite–mica stacks. Transmission electron microscopy (TEM), however, is capable of detecting the size, shape and textural relationships of small crystals in mudrocks as well as defining their structure. Moreover, analytical electron microscopy (AEM) allows chemical analysis to be directly obtained from small packets of clay minerals (as thin as 50 Å. Using these high-resolution methods, detailed textural and chemical relationships between detrital and authigenic clay minerals can be obtained. In this study chlorite–mica stacks as well as the fine-grained authigenic phyllosilicate minerals in the matrix of Llandovery slates of central Wales, U.K. have been investigated using XRD, SEM, EMPA, TEM and AEM methods in order to determine the nature and origin of the chlorite–mica stacks and other phyllosilicates and their evolution during diagenesis through very low-grade metamorphism.

PROCEDURES AND OBSERVATIONS

Material and methods of study

The sample examined for this study, BRM 1280 (NGR SN 979 688), was collected from a sequence of thinly laminated turbidite mudstones forming part of the Rhayader Mudstone Formation of Llandovery (Silurian) age (British Geological Survey 1992). A discontinuous cleavage is developed in the outcrop of pale-green mudstones, located about 1 km northeast of Rhayader (Fig. 1). The outcrop lies within an area of very low-grade (lower anchizone) regional metamorphism (British Geological Survey 1992), and the sample has a white mica (illite) crystallinity (half-height breadth of 10 Å peak; Kubler 1968) of 0.35° $\Delta 2\theta$ (Cu$K\alpha$). Within this area, depth of burial in the >5 km thick succession (Fletcher *et al.* in press), is inferred to have exercised an important control on grade (Merriman *et al.* 1992), and regional metamorphic studies of adjacent areas of the Welsh Basin similarly conclude that grade generally

correlates with the thickness of overburden (Robinson & Bevins 1986, Awan & Woodcock 1991, Roberts *et al.* 1991).

Regular polished thin sections were prepared for petrographic observation and EMPA analysis, and stickywax-mounted thin sections for TEM specimens. Thin sections were cut perpendicular to both bedding and cleavage to obtain optimum orientation for SEM observations of textural relationships and in order to obtain TEM (001) lattice fringe images of phyllosilicates. Following SEM study using back-scattered electron (BSE) imaging and X-ray energy dispersive spectral (EDS) analysis, ion-milled specimens were prepared following the method described in Li *et al.* (in revision) prior to TEM observation on a Philips CM12 scanning transmission electron microscope (STEM) fitted with a Kevex Quantum solid-state detector and computer system. The STEM was operated at an accelerating voltage of 120 kV and a beam current of ~ 10 μA. AEM quantitative chemical analyses were obtained and calculated using standards described in Li *et al.* (in revision). Chemical compositions of the coarse chlorite and mica in stacks were also determined using a Cameca CAMEBAX electron microprobe operated at 12 kV accelerating voltage and 10 nA beam current. The EMPA results are consistent with but display less variation than AEM analyses of the same materials. XRD data were obtained for the powdered bulk rock sample, using a Philips automated diffractometer with graphite monochromator and Cu$K\alpha$ radiation to define the principal minerals. Chamosite (Fe-rich chlorite), phengitic muscovite and other white micas, quartz and albite were detected.

SEM and optical observations

As seen in Figs. 2 and 3, chlorite–mica stacks are commonly 10–150 μm in longest dimension and much coarser than the grains of matrix phyllosilicates (less than 2 μm in thickness). The fine-grained matrix also consists largely of white mica and chlorite. Most stacks have packets (100 Å–8 μm thick) of white mica which are easily identified optically and by contrast in their BSE images. Chlorite packets within each grain (except within some deformed and rotated stacks) collectively constitute an optically continuous unit even though they may be separated by packets of white mica. In most cases, separate white mica packets within each stack do not constitute an optically continuous body, and their optic axes have slightly different orientations. Chlorite is usually the dominant mineral in these stacks, with white mica comprising less than 20% of the total volume, although proportions as large as 50% were occasionally observed.

The distribution of chlorite–mica stacks in slates is related to the varying depositional texture. Large grains are concentrated in the coarser-grained, lower portions of graded pelitic laminae, and the abundance and grain size of stacks gradually decrease upward (Fig. 2a). Such size distribution has also been observed by Milodowski & Zalasiewicz (1991) in slates in central Wales and by Beutner (1978) in the Martinsburg Slate. Grains of chlorite–mica stacks are usually larger than accompanying detrital quartz and albite (Fig. 2b), but the sizes of stack grains and all detrital minerals are more alike in the coarse-grained, lower portions of units. Quartz grains with angular shapes that are much larger than chlorite–mica stacks are occasionally seen in the slates (Fig. 2c). Chlorite–mica stacks are generally rectangular to ovoid in cross-section, with length to width ratios larger than 2:1, and with long dimensions parallel or subparallel to bedding. Some stacks have a subhedral or euhedral shape reminiscent of typical amphibole or pyroxene euhedra (Fig. 2d, indicated by arrow), consistent with the observations of Milodowski & Zalasiewicz (1991). Most of the chlorite–mica stacks have (001) basal planes oriented parallel or subparallel to bedding (Figs. 2b & d), implying an original bedding-parallel fabric. In slates, the primary bedding-parallel fabric of chlorite–mica stacks has been noted by many workers (e.g. Beutner 1978, Craig *et al.* 1982, van der Pluijm & Kaars-Sijpesteijn 1984, Dimberline 1986, Morad 1986), despite the commonly observed wide variation in the angle between bedding and cleavage. Usually the orientation of the stacking plane is related to bedding rather than cleavage, and where cleavage and bedding are at a high angle, (001) of stack phyllosilicates will be oriented at a large angle to cleavage.

Most of the chlorite and white mica packets in stacks are intergrown with (001) parallel or subparallel. Some mica packets have a lenticular shape or thickness that is variable (Fig. 2b) so that the number of the layers making up the thickness of mica packets must vary across the lateral dimensions of a packet requiring that boundaries with chlorite are at least partially incoherent (see below). However, the orientation of white mica in stacks may be quite variable where the spaced cleavage is well developed; for example, mica packets may be deflected from bedding toward the spaced cleavage plane (Figs. 2e & f). Chlorite–mica stacks commonly are markedly deformed, with some stacks cross-cut by cleavage (Figs. 3a–c). Bending and rotation of entire chlorite–mica stacks toward the cleavage plane, although relatively uncommon, has also been observed (Figs. 3a & c).

In most cases, intergrowths of chlorite and white mica terminate abruptly against the cleavages that cross-cut stacks (Figs. 3a & c), and the cleavage planes are deflected around the stacks and detrital-like particles. However, textures also suggest that mica packets postdate cleavage formation in some cases. For example, undeformed mica packets were observed cross-cutting a fracture plane, related to the cleavage deformation of chlorite–mica stacks (Figs. 2f and 3a). In Fig. 3(b), a grain with deformed packets is cross-cut by tabular white mica (indicated by arrow).

A small number of detrital-like coarse grains were observed to consist only of chlorite. In addition to quartz and albite, other coarse detrital-like minerals include white mica without chlorite, or with only a small amount of chlorite interleaved where subgrains are in contact

with deformed chlorite–mica stacks (Fig. 3d, indicated by arrow). SEM observations of thin sections also show the presence of other accessory phases such as titanium oxide (rutile?), apatite and zircon.

TiO_2 polymorphs were observed by SEM to occur pervasively, being easily detected by their bright contrast in BSE images. Although EDS analyses define the composition, it was not possible to identify the polymorph. We therefore refer to it simply as TiO_2, although it is most likely rutile. TiO_2 grains are 0.5–5 μm in size, with subhedral to euhedral shapes. They occur as individual grains or as small crystal clusters that are randomly distributed in the matrix. However, they are more frequently seen within chlorite in stacks, or as needle-like crystals surrounding chlorite–mica stacks (Fig. 2e). Similar distribution of rutile needles around chlorite–mica stacks was also observed in Middle Cambrian metabentonites in North Wales (Roberts & Merriman 1990).

The fine-grained mudstone matrix consists predominantly of white mica and chlorite, and subordinate quartz and albite. In contrast to the large detrital-like grains of mica and chlorite, they occur as submicroscopic grains that are usually less than 2 μm in size (thickness), with (001) oriented parallel to one of two preferred orientations: one broadly parallel to bedding in the microlithons (S_0, Q-domains) and one broadly parallel to cleavage in the relatively thin P-domains (S_1). The angle between bedding and cleavage is generally 30–50° but in some thin P-domains this angle may range up to 90° (Fig. 4). Orientation measurements of matrix phyllosilicates in such P-domains were made using BSE images with high magnifications which allow phyllosilicates <2 μm thick to be identified. The result (Fig. 5) shows that the more abundant type of matrix phyllosilicates are oriented with (001) parallel or subparallel to bedding (S_0), whereas the second, less abundant type is preferentially oriented parallel or subparallel to cleavage (S_1, e.g. Figs. 2b & f). Additionally, (001) of some fine-grained matrix phyllosilicates is subparallel to grain margins of detrital-like grains where they are adjacent to and wrap around the latter.

Transmission electron microscopy

Textural relationships. TEM images show that chlorite–mica stacks have sharply defined boundaries, characterized by the much larger packet size of phyllosilicates in the stacks compared with matrix phyllosilicates. The latter generally have (001) oriented parallel to these boundaries, so that stack layers terminate abruptly where they intersect matrix phyllosilicate layers at both high and low angles (Fig. 4). In contrast to the dominance of chlorite in stacks, white mica is the principal phyllosilicate in the matrix. Selected area electron diffraction (SAED) patterns having (001) reflections of matrix phyllosilicates confirm that basal planes of both white mica and chlorite are dominantly subparallel to sedimentary bedding.

Some matrix phyllosilicates have (001) parallel to the spaced cleavage, which is approximately 30–50° to sedimentary bedding in general, although the angle may be up to 90° in selected areas (P-domains, e.g. Fig. 4). There is a range of orientations of bedding-parallel and cleavage-parallel matrix phyllosilicates, as is typical of shales and slates. For example, Fig. 4 illustrates fan-shaped arrays of subparallel packets which have orientations ranging over several tens of degrees. However, few grains have orientations intermediate between the bedding-parallel and cleavage-parallel phyllosilicates in such thin P-domains. Similar observations were made by Lee *et al.* (1986) in rocks showing incipient cleavage development.

Five different modes of occurrence of white micas can be distinguished: (1) white mica in chlorite–mica stacks; (2) chlorite-free white mica grains with detrital-like shape; (3) matrix white mica parallel to bedding; (4) matrix white mica parallel to cleavage; and (5) white mica cross-cutting stacks. In addition, three modes of chlorite occurrence are recognized: (1) chlorite in stacks; (2) bedding-parallel matrix chlorite; and (3) cleavage-parallel matrix chlorite. Texture, polytypism and composition for each type is summarized in Table 1.

Chlorite–mica stacks. Lattice fringe images of typical chlorite–mica stacks exhibit packets of dominant 14 Å chlorite layers interleaved with packets of white mica. Such packets are commonly parallel, with boundaries that appear to be coherent, i.e. c^* of chlorite packets is parallel to c^* of the adjacent white mica packets. In other cases layers of mica and chlorite are subparallel, with mica layers terminating against a continuous layer of chlorite (Fig. 6). Such incoherent relations are con-

Table 1. Summary of textural and mineralogical characteristics of phyllosilicates in a cleaved mudstone from Central Wales, U.K.

	Grain size (thickness)	Defect	Polytypism	Composition
Mica in stacks	100 Å–8 μm	absent	$2M_1$	phengitic muscovite
Mica cutting stacks	100 Å–4 μm	absent	$2M_1$	muscovite
Detrital-like mica	10–40 μm	absent	$2M_1$	muscovite, paragonite ss*
Bedding-parallel mica	50 Å–2 μm	present	$2M_1$, $1M_d$	intermediate Na/K mica
Cleavage-parallel mica	100 Å–2 μm	absent	$2M_1$, $3T$	phengite and paragonite
Chlorite in stacks	100 Å–30 μm	absent	one-layer	relatively high Fe
Bedding-parallel chlorite	100 Å–1 μm	present	one-layer	relatively low Fe
Cleavage-parallel chlorite	100 Å–0.5 μm	absent	one-layer	intermediate Fe

*ss: solid solution.

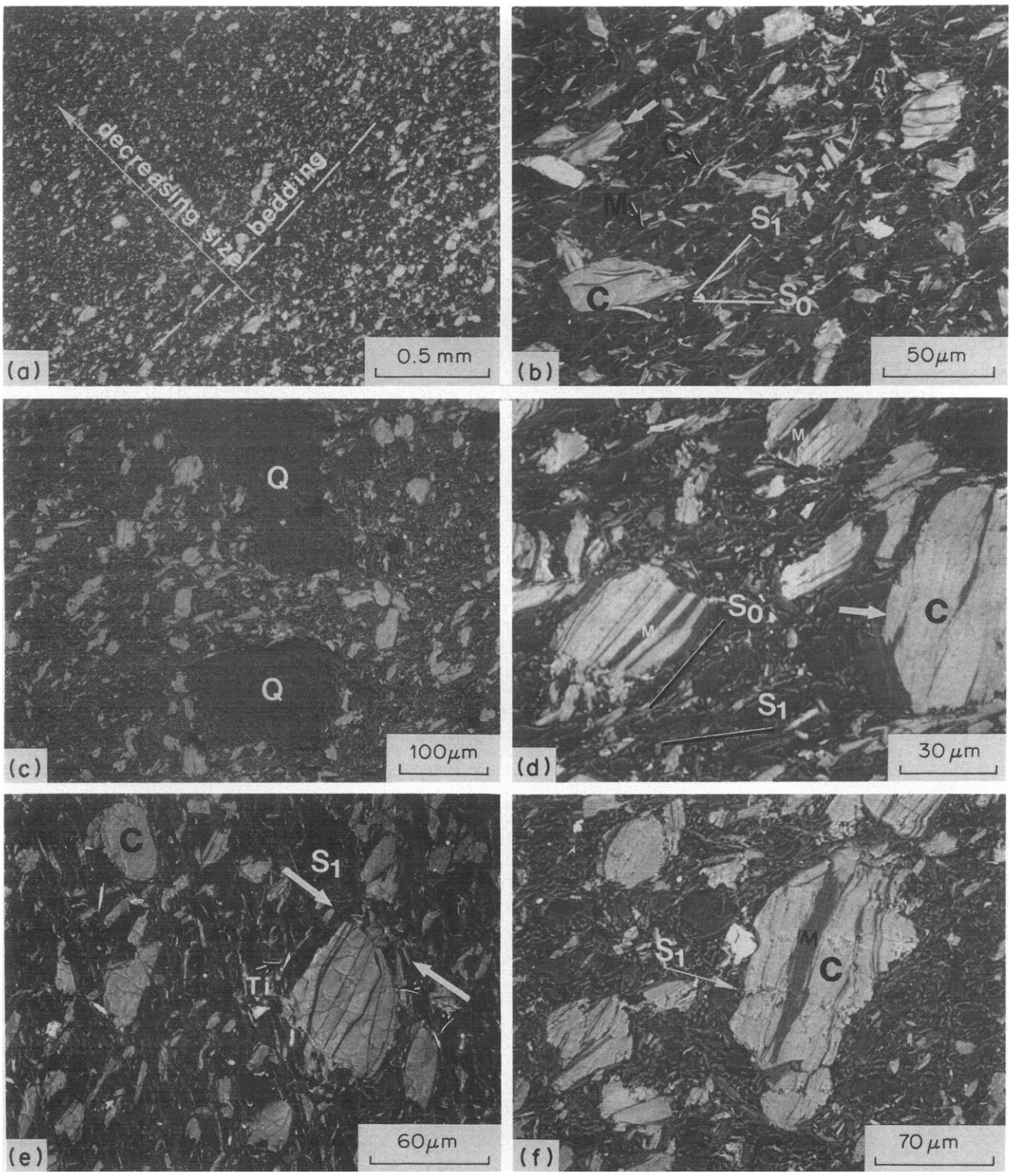

Fig. 2. Back-scattered electron (BSE) images showing textures of chlorite–mica stacks in a cleaved mudstone. (a) Distribution of chlorite–mica stacks in a single pelitic lamina. The size of stacks decreases from the bottom of the unit upward. (b) The sizes of stacks are usually larger than those of quartz and albite detrital grains. The basal planes of phyllosilicates in stacks and fine-grained matrix phyllosilicates are mostly parallel to bedding, but some stacks (indicated by a white arrow) are oriented with basal planes at high angle to bedding. (c) Angular detrital quartz grains much larger than chlorite–mica stacks are occasionally seen in slates. (d) Chlorite and white mica in stacks are intergrown parallel or subparallel to their (001) planes, which in turn are parallel to bedding. Some stacks have crystal shapes resembling amphibole or pyroxene euhedra. (e) Some mica packets in stacks are curved toward cleavage, and some phyllosilicates in the matrix are parallel to cleavage. TiO_2 crystals (indicated by thin arrows) were observed surrounding chlorite–mica stacks. (f) Mica intergrowths in stacks cutting across a cleavage induced fracture which cross-cut the stacks. (C) chlorite, (M) white mica, (Q) quartz, (Ti) titanium oxide, (S_0) sedimentary bedding, (S_1) spaced cleavage.

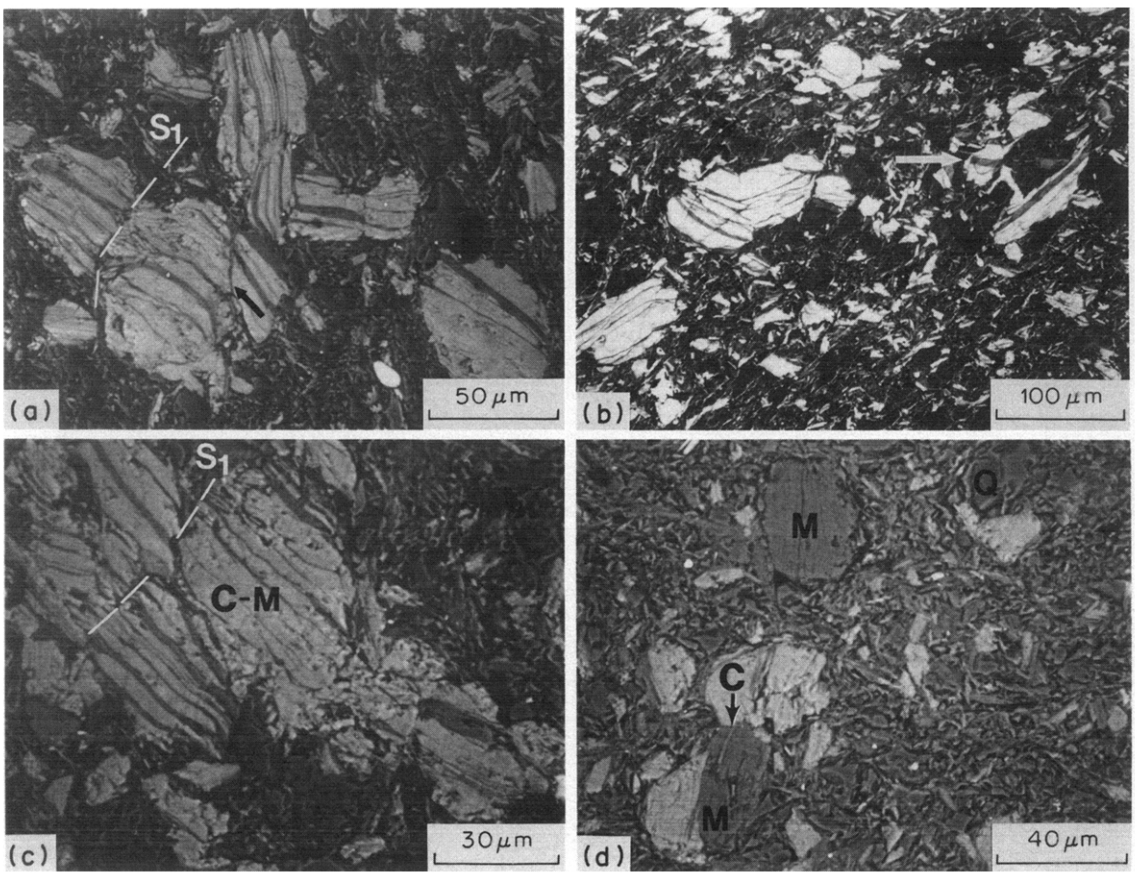

Fig. 3. BSE images showing texture of chlorite–mica stacks in a cleaved mudstone. (a) White mica (indicated by arrow) transecting earlier-formed mica in stacks, forming anastomosing networks of mica intergrowths. Rotation, bending and kinking of the stacks occurred near cleavage planes. (b) A later tabular mica (indicated by an arrow) cross-cuts a folded stacks grain. (c) Intergrowths of chlorite–mica in the stacks terminate abruptly at cleavage planes. (d) Detrital white mica grain without interleaved chlorite, and one with a small amount of chlorite (indicated by arrow). The latter is in contact with chlorite–mica stacks which were affected by cleavage formation and fractured along with the white mica grain. (C) chlorite, (M) white mica, (C–M) chlorite–mica stacks, (Q) quartz, (S_0) sedimentary bedding, (S_1) cleavage.

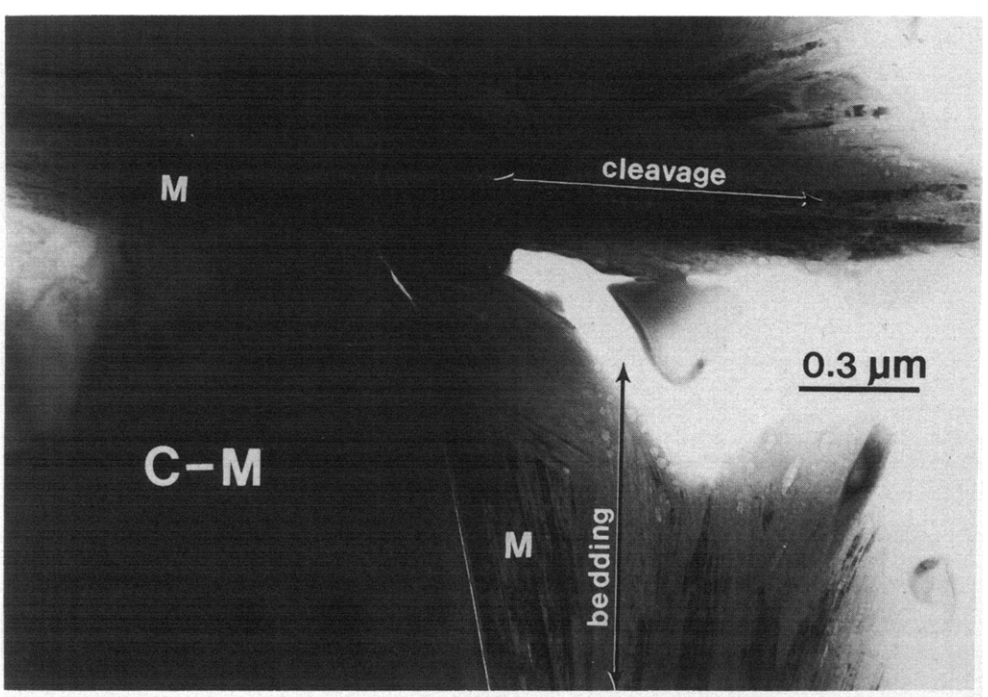

Fig. 4. TEM image showing part of the sharp boundary of a chlorite–mica stack (C–M). Surrounding thin matrix phyllosilicate packets (M) terminate abruptly at its margin whether oriented at high angles or subparallel to the basal plane of thick phyllosilicates packets in stacks; the latter are approximately parallel to sedimentary bedding.

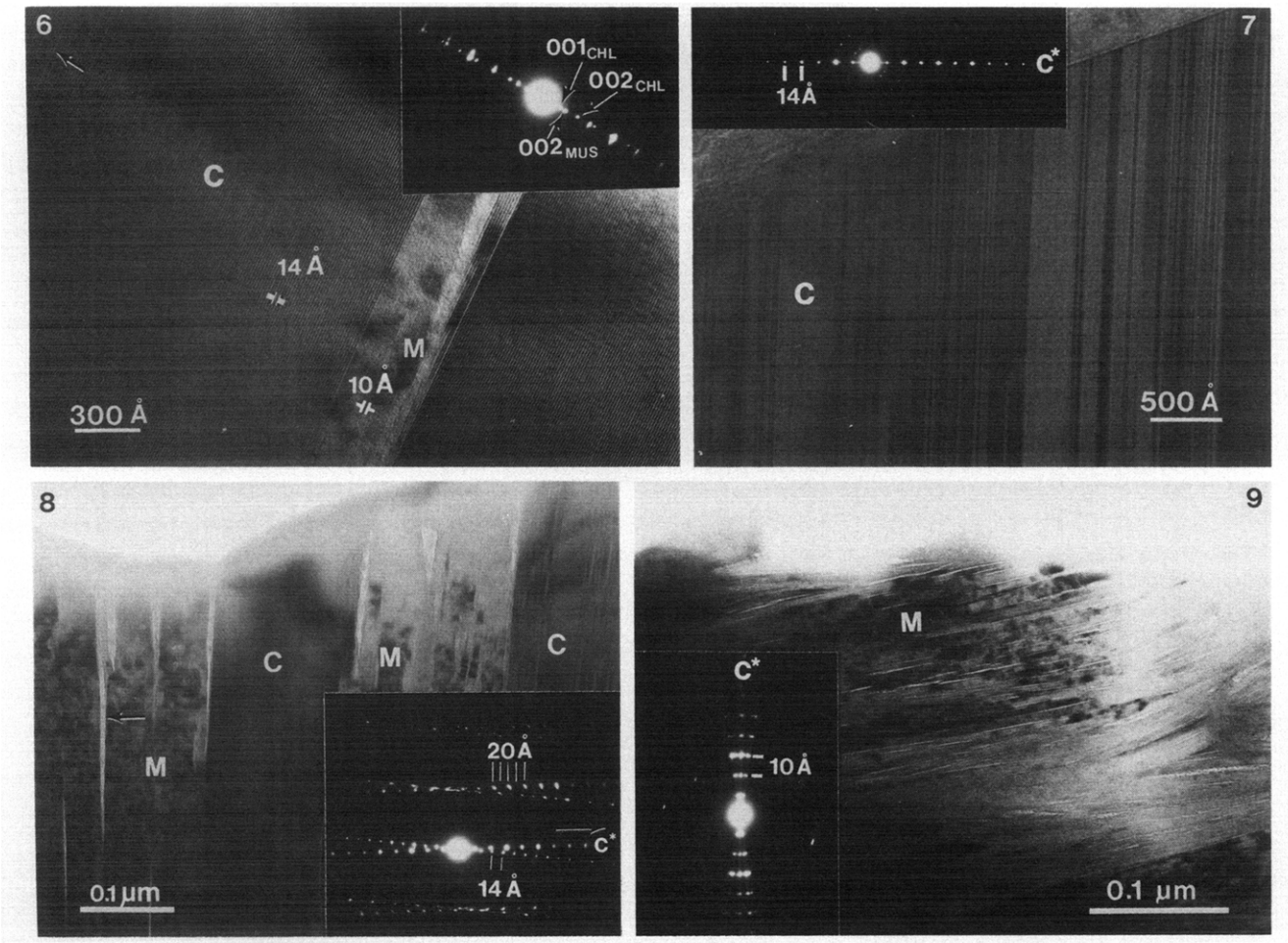

Fig. 6. TEM lattice fringe image of intergrowth of white mica and chlorite in stacks, the inset selected area electron diffraction (SAED) pattern showing that (001) layers of each are subparallel. Chlorite has a highly perfect structure with well-developed packets of several 1000 Å thick, with only a few defects (indicated by an arrow) observed within hundreds of layers. (C) Chlorite, (M) white mica.

Fig. 7. TEM lattice fringe image of chlorite (C) in stacks displaying variable contrast due to layer-stacking disorder, consistent with the diffuse streaking along c^* in the inset SAED pattern

Fig. 8. TEM lattice fringe image displaying adjacent white mica (M) intergrowths with subparallel chlorite (C) layers in chlorite-mica stacks. The inset SAED pattern shows two-layer polytypism of white mica.

Fig. 9. TEM lattice fringe image of fine-grained bedding-parallel matrix white mica (M) showing bending and various defects such as dislocations and low-angle boundaries. The inset electron diffraction pattern shows that it is a disordered 1 M_d polytype with streaking along c^*.

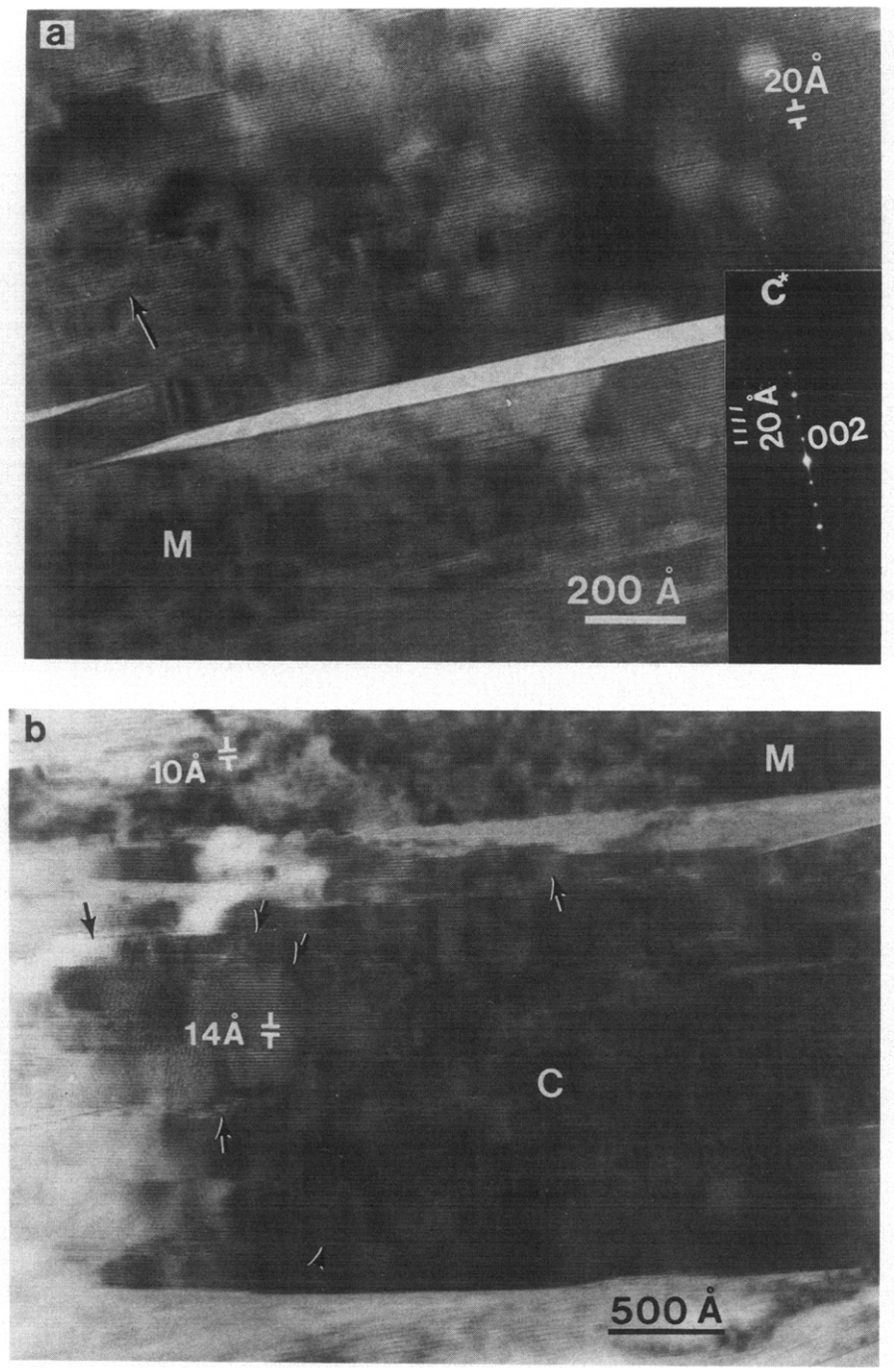

Fig. 10. (a) TEM lattice fringe image of relatively coarse-grained matrix white mica (M) demonstrating its relatively defect-free nature. Lenticular splitting along layers is due to beam damage during TEM observation. The inset electron diffraction pattern shows that it is a well-crystallized two-layer polytype. (b) TEM lattice fringe image of bedding-parallel chlorite (C) coexisting with white mica (M) in the matrix shows various defects and deformation features such as layer terminations, edge dislocations, kinking and bending (indicated by arrows).

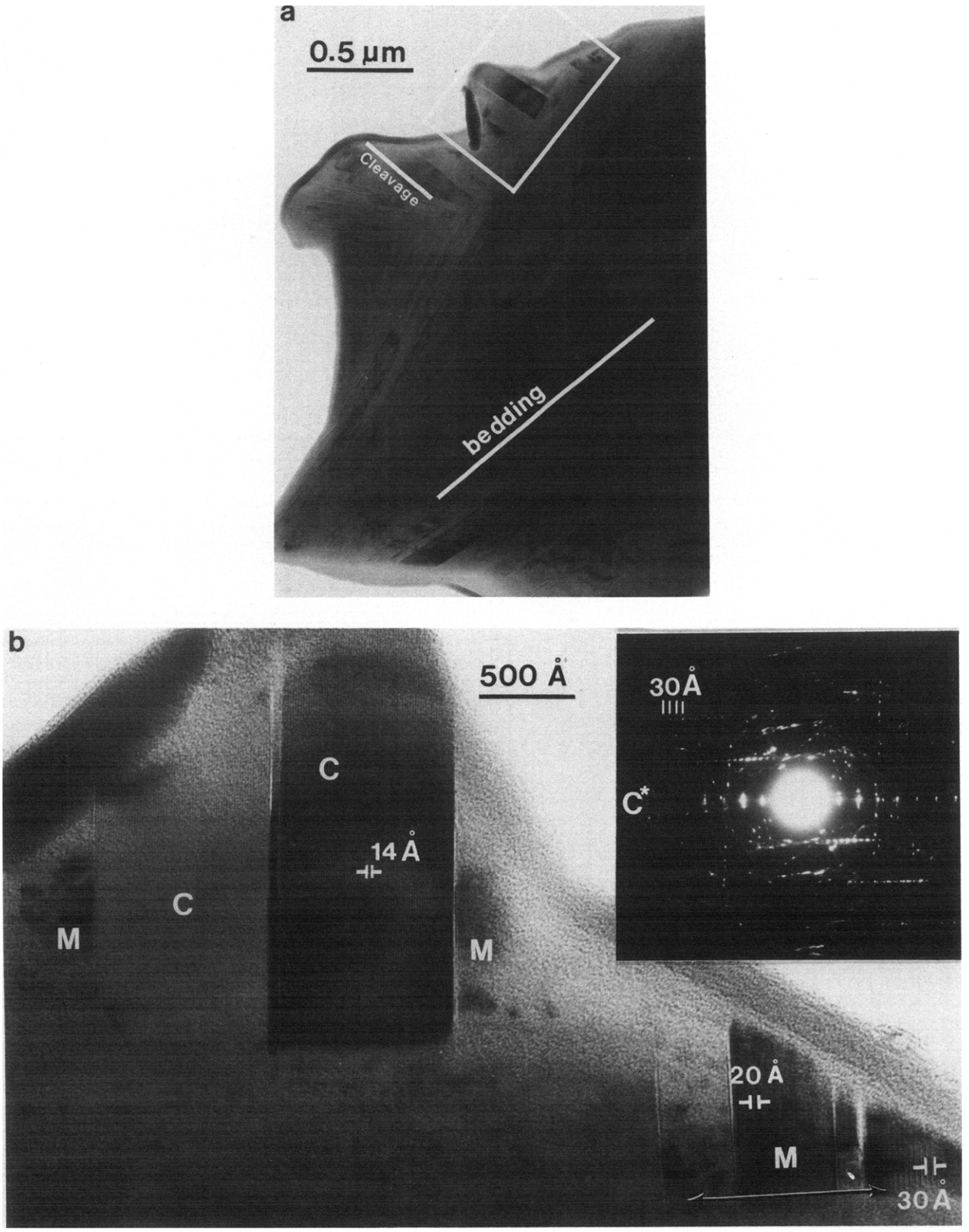

Fig. 11. TEM images of euhedral to subhedral cleavage-parallel white mica and chlorite crystals occurring in the matrix. (a) A low magnification bright field image showing euhedral to subhedral white mica (M) and chlorite (C) oriented approximately normal to bedding. (b) An enlargement of part (a). Platy subhedral white mica crystals are two- and three-layer polytypes, and platy euhedral-to-subhedral chlorite displays defect-free fringes with 14 Å periodicity.

sistent with the variable mica packet thicknesses observed by SEM.

Chlorite occurs as well-developed packets several thousand angstroms thick, having highly perfect structure; very few defects, such as layer terminations (indicated by an arrow in Fig. 6), were observed in packets consisting of hundreds of layers. Chlorite packets of coherent layers commonly display variable contrast (Fig. 7). Such contrast results from stacking faults that are also indicated by diffuseness parallel to c^* in SAED patterns (insert in Fig. 7). No mixed-layering of mica was observed within packets of chlorite.

Individual packets of white mica interleaved with chlorite packets range from a few 10s to a few 100s Å thick, with a collective thickness of up to several 1000 Å in a given stack. Lattice fringe images of packets of white mica generally display parallel, defect-free, coherent layers; layer terminations are rarely observed. No chlorite was observed to be mixed-layered with mica.

In some cases, adjacent white mica packets, each of which appear to be defect-free, display subparallel boundaries with elongate lenticular fissures which are probably an artifact of beam damage (Fig. 8). The 'mottled' structure displayed in lattice fringe images of white mica is characteristic of cation diffusion induced by the electron beam (Ahn & Peacor 1986). SAED patterns (e.g. inset in Fig. 8) suggest that most of the white mica is well-crystallized, and consists of a two-layer polytype (presumably $2M_1$). Slight diffuseness parallel to c^* was occasionally observed in some SAED patterns, probably due in part to the presence of the interpacket beam damage.

White mica in matrix. Bedding-parallel white mica consists of both fine-grained deformed crystals (≤200 Å thick) and coarse-grained undeformed crystals (up to 2 μm in thickness). Cleavage-parallel white mica (100 Å–2 μm in thickness) is relatively undeformed and sometimes occurs as discrete crystals with platy subhedral shapes.

The smallest crystals of matrix bedding-parallel white mica, 50–200 Å thick, occur as subparallel packets bordered by low-angle grain boundaries, and contain high concentrations of layer terminations. Kinked, bent, and curved layers are frequently observed, and they are associated with lenticular voids between layers (Fig. 9). These strain features show that the small white mica crystals are highly deformed. Electron diffraction patterns confirm that such white mica is a disordered $1M_d$ polytype with 10 Å periodicity (inset in Fig. 9), although some grains are a two-layer polytype, but with streaking along c^* representing stacking disorder.

Relatively coarse-grained crystals of white mica in the bedding orientation occur as well-defined packets of layers that display little or no deformation. Such packets are oriented parallel or subparallel to each other, and appear to be relatively defect-free, with layer terminations being rarely observed (Fig. 10a, indicated by arrow). The 'mottled' structure and lenticular fissures along layers in this example are in part due to beam damage. Relatively coarse-grained white mica displays (00*l*) lattice fringe periodicities of *ca* 10 and 20 Å, and the SAED pattern in Fig. 9 shows that the white mica is a well-crystallized, two-layer polytype ($2M_1$). Streaking along c^* is also observed in SAED patterns. Although most electron diffraction patterns of coarse-grained bedding-parallel white mica only show a single, well-defined sequence with 20 Å periodicity, one of them was observed to have unusual satellite reflections with rational indices relative to those corresponding to 20 Å periodicity (Li *et al.* in revision). This type of structure is referred as a commensurate modulation since the superstructure spots are rational multiples of the substructure (Buseck & Cowley 1983) and is inferred to be due to ordering of interlayer Na and K.

The white mica oriented parallel to cleavage is generally similar to the more coarse-grained white mica in the bedding orientation; that is, it is relatively defect-free and is dominantly a two-layer polytype ($2M_1$). Occasionally, electron diffraction patterns of such cleavage-parallel mica show weak reflections of paragonite associated with strong reflections of muscovite. Such reflections show that both muscovite and paragonite coexist as well-defined two-layer polytypes. Intergrown paragonite and white mica packets were also detected with electron diffraction patterns, but not in lattice fringe images from an anchizonal slate sample from north Wales (Merriman *et al.* 1990). Some cleavage-parallel white mica was observed to have an uncommon morphology consisting of platy individual crystals 100–1000 Å thick (Fig. 11). It consists of straight, defect-free layers that are parallel to the (00l) boundaries. Similar crystal shapes, considered to represent cross-sections of euhedral to subhedral hexagonal crystals, have been imaged in illites in shales from Salton Sea geothermal field, where they formed by direct crystallization from convected fluids (Yau *et al.* 1987b); in illite in Triassic volcanogenic sediments from the Southland Syncline, New Zealand (Ahn *et al.* 1988); and in illite synthesized under hydrothermal conditions (Yau *et al.* 1987a). Such crystals are therefore inferred to be subhedral in morphology but further observation in three-dimensions need to be made using clay separates. Although two-layer polytypes were ubiquitously observed in other crystals, here the material consists of both two- and three-layer polytypes (Fig. 11b, an enlargement of part of Fig. 11a).

Chlorite in matrix. Matrix chlorite is subordinate to white mica. It occurs as well-defined packets of layers that are almost always closely associated with white mica. Although the thickness of chlorite packets varies, most are less than 2 μm thick and are occasionally as thin as 100 Å. As is the case for white mica, matrix chlorite has two distinctly different orientations, parallel to bedding and parallel to cleavage. Bedding-parallel chlorite also consists of both relatively coarse-grained (300 Å–2 μm) and undeformed crystals, and relatively fine-grained (<200 Å) and deformed crystals. Cleavage-parallel chlorite was never observed to have defor-

mation features, but occurs as discrete subhedral crystals.

Lattice fringe images of coarse-grained bedding-parallel chlorite commonly show straight, coherent layers with 14 Å periodicity which are relatively defect-free; layer terminations are rarely observed. However, fine-grained chlorite is quite different. For example, a lattice fringe image (Fig. 10b) of fine-grained chlorite coexisting with white mica shows that low-angle boundaries occur both between chlorite packets and between chlorite and white mica crystals. Crystal defects such as edge dislocations, layer terminations and layer splitting are also commonly observed, features which suggest that the small crystals have been deformed. Matrix chlorite parallel to cleavage is generally undeformed and defect-free, similar to cleavage-parallel white mica. Discrete, subhedral crystals of chlorite are observed in association with subhedral white mica crystals (Fig. 11b). Packets of straight, coherent, defect-free chlorite layers may be up to 800 Å thick, and are oriented parallel or subparallel to adjacent chlorite and subhedral white mica crystals. Such chlorite crystals have also been observed in association with euhedral to subhedral illite crystals in shales from the Salton Sea geothermal field (Yau *et al.* 1987b); and in Triassic volcanogenic sediments from the Southland Syncline, New Zealand (Ahn *et al.* 1988).

White mica in detrital-like grains. Large flakes of detrital-like white mica consist of aggregates of parallel to subparallel packets, each ranging from a few 100 to 1000 Å in thickness. SAED patterns show that they consist of well-crystallized two-layer polytypes. There is less diffuseness along c^* of the SAED patterns, compared with those of white mica in the matrix.

Analytical electron microscopy

AEM data were normalized on the basis of 12 tetrahedral and octahedral cations for white mica and 14 O-atoms for chlorite. Average compositions of the various types of white mica and chlorite are given in Tables 2 and 3. Although the various types of white mica differ in ways described above, most have compositions approaching those of evolved micas, with net negative charges close to 2 per formula unit (pfu); i.e. the net negative charges are typical of those of phengite or muscovite rather than authigenic illite, for which net negative charges are considerably smaller (≈1.6, Środoń *et al.* 1986).

White mica in stacks and detrital-like grains. The structural formulae (Table 2, analyses 1–4) of most white mica in chlorite–mica stacks are similar to those reported for mica in stacks of other Paleozoic turbidites (Craig *et al.* 1982, Dimberline 1986, Milodowski & Zalasiewicz 1991). They are generally phengitic in composition, having higher Si/Al ratios (6.20–6.35 Si pfu) than muscovite and with significant Fe and Mg. The Fe/(Mg+Fe) ratio varies over a wide range (0.3–0.85). The micas display slight deficiencies in interlayer cations (K+Na+Ca = 1.83–1.94) but are still within the range of typical mica; that is, they have 'mature' compositions as compared with authigenic illite. The Na/(K+Na+Ca) ratio is less than 0.1 in general, and no Na is detectable in some analyses. On the other hand, the detrital-like grains consisting only of white mica have Si and Al contents (Table 2, analysis 5) similar to those of end-member muscovite. Their Fe and Mg contents are much lower than those of white mica in stacks, and there is significant Na (up to 0.32 pfu) present.

Both the white mica in chlorite–mica stacks and the detrital-like white mica contain Ti, the amount in the mica in chlorite–mica stacks (0.04–0.11 pfu) being greater than that in the detrital-like white mica (0.3 pfu). Although measurable Ti contents are common in trioctahedral micas they are unusual in dioctahedral micas. Special care was therefore taken to ensure that analyses were obtained from areas shown by TEM to consist only of white mica, with no adjacent Ti-containing minerals such as rutile. Such observations verify that Ti is present in solid solution.

White mica in matrix. The average compositions (cf. table 1 in Li *et al.* in revision) of bedding-parallel matrix white mica show high Na contents [Na/(Na+K+Ca) ~0.14–0.42]. The high Na contents are incompatible with the wide solvus in the system muscovite–paragonite (e.g. Eugster 1956, Eugster *et al.* 1972, Blencoe & Luth 1973), and attempts to determine the spatial distribution of Na and K were therefore made. Compositions with high Na were frequently obtained in fine-grained and deformed bedding-parallel micas even using a point beam with a 50 Å diameter, suggesting the presence of disordered intermediate Na/K mica, consistent with single diffraction patterns observed in such materials. The Na/(Na+K+Ca) ratios from adjacent areas are quite variable. The probable occurrence of interlayered Na- and K-rich layers would require diffuseness in (00*l*) reflections, especially when the non-(00*l*) reflections that are a measure of stacking sequence are excluded. Such diffuseness was commonly observed. In addition, the occurrence of the modulated structure as indicated by irrational (00*l*) reflections in the white mica having a relatively high Na content [Na/(Na+K+Ca) = 0.29] is also consistent with local ordering of Na- and K-rich layers.

The range of Fe+Mg contents in bedding-parallel white mica in the matrix is similar to that of detrital-like white mica, but both types have Fe contents much smaller than those of white mica in chlorite–mica stacks. Bedding-parallel white mica differs, however, from the detrital-like white mica in having relatively low total interlayer cations (~1.75 pfu), especially in relatively fine-grained and deformed white mica parallel to bedding (~1.66 pfu, as consistent with its $1M_d$ polytypism. The Ti content (0.01–0.02 pfu) of white mica in the bedding orientation is generally relatively low compared to that of white mica in chlorite–mica stacks.

Although some white mica with significant Na was

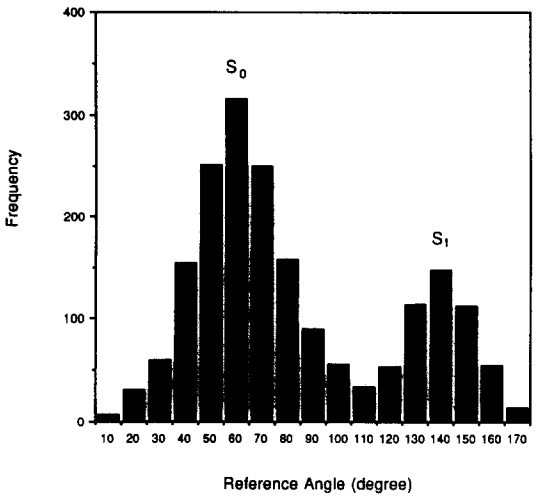

Fig. 5. A histogram showing orientation of (001) of fine-grained phyllosilicates in the matrix as measured on BSE images of some thin *P*-domains. (S_0) sedimentary bedding, (S_1) cleavage.

Table 3. Normalized AEM data for chlorite*†

	1	2	3	4	5	6
Si	2.58	2.56	2.57	2.60	2.58	2.56
Al^{IV}	1.42	1.44	1.43	1.40	1.42	1.44
Al^{VI}	1.53	1.53	1.61	1.52	1.55	1.53
Ti	n.d.‡	n.d.	n.d.	n.d.	n.d.	n.d.
Fe^{2+}	3.40	3.32	2.97	3.02	3.13	3.20
Mg	0.95	1.07	1.32	1.38	1.23	1.19
Mn	0.06	0.03	0.05	0.02	0.04	0.03
Total cations	9.94	9.95	9.95	9.94	9.96	9.95
Fe/Fe + Mg	0.78	0.76	0.69	0.69	0.72	0.73

*Each formula is normalized on the basis of 14 O-atoms and is an average of at least six scanning areas within the same grain, and all Fe calculated as FeO. Two standard deviations on the basis of calculating statistics are 0.05–0.07 pfu for Si, 0.03–0.04 and 0.04–0.05 pfu for Al^{IV} and Al^{VI}, respectively, 0.20–0.25 pfu for Fe, 0.09–0.15 pfu for Mg and 0.01–0.02 pfu for Mn.

†Analyses 1 and 2 were derived from chlorite in stacks, while 3 and 4 and 5 and 6 were from matrix chlorite parallel to bedding and cleavage, respectively.

‡n.d. = not detectable.

Table 2. Normalized AEM data for white mica in detrital grains*†

	1	2	3	4	5
Si	6.24	6.25	6.22	6.31	6.01
Al^{IV}	1.76	1.75	1.78	1.69	1.99
Al^{VI}	3.56	3.54	3.59	3.32	3.84
Ti	0.04	0.06	0.07	0.11	0.03
Fe^{2+}	0.34	0.13	0.14	0.16	0.05
Mg	0.06	0.27	0.20	0.41	0.08
Ca	0.04	n.d.‡	n.d.	n.d.	n.d.
Na	0.13	0.13	n.d.	n.d.	0.32
K	1.75	1.76	1.83	1.94	1.58
Total cations	13.92	13.89	13.83	13.94	13.90
Na/(K + Na + Ca)	0.068	0.069	0	0	0.168

*Each formula is normalized on the basis of 12 cations on tetrahedral and octahedral sites and is an average of at least six scanning areas within the same grain, and all Fe calculated as FeO. Two standard deviations on the basis of calculating statistics are 0.11–0.15 pfu for Si, 0.04–0.05 and 0.08–0.09 pfu for Al^{IV} and Al^{VI}, respectively, 0.01–0.02 pfu for Ti and Ca, 0.01–0.03 pfu for Fe 0.01–0.05 pfu for Mg, 0.02–0.04 pfu for Na and 0.10–0.14 pfu for K.

†Analyses 1–4 and 5 were derived from white mica in chlorite–mica stacks and detrital white mica, respectively.

‡n.d. = not detectable.

also detected in cleavage-parallel orientation, cleavage-parallel white micas in the matrix generally have compositions with very high concentrations of K and Na, respectively, consistent with the split reflections in their SAED patterns which indicate coherent diffraction of two separate phases (Li *et al.* in revision). The Na white mica has a ratio of Si/Al ~1 and the normalized formula corresponds to near end-member paragonite (Mu_6Pg_{94}), whereas the K white mica has a larger Si/Al ratio with more (Fe+Mg) and its normalized formula corresponds to phengitic muscovite. The compositions of cleavage-parallel white mica are intermediate to those of bedding-parallel white mica in the matrix and those of white mica in stacks, but the Na content is more like the former and the (Fe+Mg) components more like the latter. In comparison with white mica parallel to bedding, cleavage-parallel white mica has a smaller deficiency in interlayer cations (1.80–1.85 pfu).

Chlorite. Chlorite (Table 3) has a high Fe(Fe+Mg) ratio (0.69–0.78), and is best described as chamosite (Bayliss 1975). Such Fe-rich chlorite of diagenetic origin in sedimentary rocks has been observed by many other workers (e.g. Hayes 1970, Lee *et al.* 1984, Curtis *et al.* 1985, Dimberline 1986, Milodowski & Zalasiewicz 1991). The formulae of chlorite show a large range of excess Al^{VI} (0.06–0.18 pfu) over Al^{IV}, and this is characteristic of low-grade metamorphic chlorite in clastic sedimentary rocks (Boles & Coombs 1977, Ramamohana Rao 1977, Evarts & Schiffman 1983, Weaver 1984, Morad 1986, Aguirre & Atherton 1987), and has been related to the amount of interlayered expandable material by Shau *et al.* (1990).

Bedding-parallel matrix chlorite has the lowest Fe/(Fe+Mg) ratio whereas chlorite in stacks has the highest ratio (see Table 3). On the other hand, the Mg content of matrix chlorite in the cleavage orientation is slightly richer than that of chlorite in stacks and poorer than that of matrix chlorite in the bedding orientation, and has an Fe/(Fe+Mg) ratio intermediate between the two. Minor Mn (0.02–0.06 pfu) was also detected in all types of chlorite.

DISCUSSION

Observations of detailed crystal structural and chemical relations of the various phyllosilicates in the studied sample place constraints on the formation of chlorite–mica stacks, the nature of precursors, alteration mechanism, and interaction between chlorite–mica stacks and matrix phyllosilicates. These topics will be discussed in the following sections.

Origin of chlorite–mica stacks

Textural relationships between chlorite–mica stacks and the spaced cleavage suggest that the stacks were present prior to or early in the development of the cleavage. The pre- to early cleavage origin of the stacks has been recognized by many workers (Frey 1970, 1978, White & Knipe 1978, Craig *et al.* 1982, Woodland 1982, 1985, van der Pluijm & Kaars-Sijpesteijn 1984, Dimberline 1986, Milodowski & Zalasiewicz 1991). The size distribution and morphology of chlorite–mica stacks, and their general parallelism with bedding (Milodowski & Zalasiewicz 1991) collectively lead to the conclusion that stacks originated from detrital-like grains.

The majority of the stacks in this study were observed to be in hydrodynamic equilibrium with the largest associated quartz and feldspar clasts (see also Dimberline 1986, Milodowski & Zalasiewicz 1991), especially at the bottom of sedimentary units, a property consistent with a detrital origin. As suggested by Milodowski & Zalasiewicz (1991), the more rapid decrease in quartz and feldspar clast sizes and populations toward the top of the turbidite units relative to the size of stacks can be explained in part by the slower settling rates of micaceous detrital grains due to greater buoyancy. In addition, irregular detrital quartz grains much larger than stacks are occasionally observed (Fig. 2c), indicating that the largest quartz clasts associated with stacks may be larger than those observed by other workers, who argued that sizes of quartz and feldspar are too small compared with those of stacks (e.g. Craig *et al.* 1982, Pye & Krinsley 1983). Craig *et al.* (1982) and Pye & Krinsley (1983) rejected an altered detrital origin because of the complexity of intergrowths of chlorite and mica. In fact, intergrowths of chlorite and white mica as complex as those observed by Craig *et al.* (1982) have been seen in diagenetically altered biotite in shales, siltstones and sandstones (Morad 1986), and in sedimentary and metamorphic rocks described by White *et al.* (1985). Furthermore, deformation textures such as kinking, bending, and cleavage cross-cutting stacks (e.g. Milodowski & Zalasiewicz 1991) also increase the complexity of the intergrowths. The complexity of chlorite–mica intergrowths, therefore, is very likely the result of alteration of detrital grains through a combination of diagenetic, metamorphic and tectonic events.

Indirect evidence of the detrital origin of the chlorite–mica stacks is provided by the differing compositions of white mica and chlorite in stacks compared with those of white mica and chlorite in the matrix. This evidence suggests that the stacks formed at different times from a very different precursor bulk composition from those of phyllosilicates in the matrix, and clearly discounts the conclusion that stacks are a mimetic replacement of clay minerals such as smectite (Craig *et al.* 1982, Woodland 1982, 1985). These compositional differences reflect several limits to diffusion such as diffusion distances, and hence the size of 'equilibration' domains controlled by the low temperature of late diagenesis and very low-grade metamorphism. In addition, detrital-like white mica which is not intergrown with chlorite is homogeneous muscovite with a significant paragonite component in solid solution, implying that it does not have a direct relationship with formation of mica in chlorite–mica stacks. If stacks originated as chlorite overgrowths on detrital micas (e.g. Voll 1960, van der Pluijm & Kaars-Sijpesteijn 1984), white mica intergrowths in stacks would also contain a considerable paragonite component, but this is not the case; white micas in stacks are phengitic in composition with much less Na than detrital-like white micas.

The data presented indicate that chlorite–mica stacks, derived from a detrital precursor, have undergone considerable textural change in response to diagensis and very low-grade metamorphism. As observed from SEM images, early-formed chlorite–mica intergrowths in stacks are truncated along the cleavage, and some mica interlayers in stacks have been folded (see also van der Pluijm & Kaars-Sijpesteijn 1984, Dimberline 1986, Milodowski & Zalasiewicz 1991). Some late white mica containing much less Fe than pre-existing white mica in stacks, cross-cuts the cleavage within stacks and is undeformed. However, TEM observations show little evidence of intracrystalline strain features within chlorite–mica stacks, in contrast to the stack deformation displayed by BSE images, and therefore imply considerable internal modification of the deformed crystal structure. Internal modification of the chlorite–mica stacks also appears as homogenized phyllosilicate compositions. For example, chlorite in stacks has an Fe-rich composition with a range of excess Al^{VI} over Al^{IV}, characteristic of a diagenetic origin. It is homogeneous chamosite with only a small range of composition. In addition, white mica in stacks is a relatively homogeneous phengitic muscovite with a very small amount of paragonite component and is a $2M_1$ polytype which is characteristic of mature white mica. Such limited ranges in chemical compositions of both chlorite and white mica suggests that the mineralogy of the stacks is the result of equilibrium conditions attained during diagenesis and very low-grade metamorphism, with such a process having been facilitated by exchange with fluids. We therefore infer that intergrowths of chlorite and white mica in stacks are due to alteration of an original detrital precursor during late diagenetic to early metamorphic processes prior to tectonism and cleavage formation. The fact that the packets of intergrown chlorite and mica in stacks are significantly larger than those occurring as matrix phyllosilicates (Table 1) suggests that, to some extent, packet size may have been inherited from a phyllosilicate precursor.

Nature of precursor and alteration mechanism

No relict phases are seen in SEM and TEM images of chlorite–mica stacks, suggesting complete alteration of the detrital precursor during diagenesis and very low-grade metamorphism. However, abundant titanium oxide grains are found within chlorite in stacks or surrounding the chlorite–mica stacks, but are less common

in other areas. In addition, white mica in stacks is unusual in having considerable Ti, whereas detrital-like white mica and matrix white mica have the low Ti contents typically found in white micas. The significant Ti content of volcanic biotite suggests that it is a probable precursor of much of the stack chlorite, as proposed by previous studies. For example, remnants of biotite were observed in chlorite–mica stacks in slates in central Wales by Dimberline (1986) who showed that the chemical compositions of igneous biotite and the average chlorite–mica stacks are similar. Remnant biotite has also been found in stacks in many other sedimentary rocks that have undergone very low- and low-grade metamorphism (e.g. Williams 1972, Weaver 1984, AlDahan & Morad 1986, Morad 1986, 1990). Jiang (1993) observed TiO_2 grains in direct association with corrensite and chlorite that largely replaced biotite of volcanic origin in low grade sediments of the Gaspé Peninsula, Québec. Detrital biotite grains in prehnite–pumpellyite facies metagreywackes from South Island, New Zealand, were found to have intergrowths of chlorite and phengite in variable proportions, with sphene sometimes forming clusters within or aligned along the interfaces between chlorite and phengite (White *et al.* 1985). Grubb & Peacor (unpublished data) observed both rutile and sphene directly associated with partial alteration of biotite in volcanoclastic rocks from New Zealand. Jiang (1993) has shown that for sediments in Québec, chlorite occurring as a major component of pelites may be derived on a massive scale through alteration of volcanic biotite. Although a likely precursor of the chlorite–mica stacks, therefore, was primarily volcanic biotite, some stacks have euhedral or subhedral shapes resembling amphibole or pyroxene minerals which, if volcanogenic, may also contain considerable Ti. Therefore, the precursor minerals of the stacks may also have included an unknown proportion of amphibole or pyroxene (Milodowski & Zalasiewicz 1991). The precursor minerals for stack development were probably derived from the volcanogenic detritus which forms a substantial part of the sediment input to the Welsh Basin (Roberts & Merriman 1990). Although volcanicity within the Welsh Basin had ceased by the end of the Caradoc (Howells *et al.* 1991), there is abundant evidence in the form of thin bentonite beds in Silurian strata (Teale & Spears 1986, Huff & Morgan 1989), that volcanic activity continued in regions adjacent to the basin. However, since the stacks occur predominantly in turbidites, reworked volcanic detritus (as opposed to airborne ash) must have supplied the bulk of the precursor material for stack development. Studies of paleocurrent directions indicate that this detritus were derived mainly from sources to the east and southeast of the central Welsh Basin during the Llandovery (Fletcher *et al.* in press). A possible source was the calc-alkaline volcanic arc of probable Ordovician age which is now concealed beneath eastern England (Pharaoh *et al.* 1991).

Direct alteration of biotite to chlorite during diagenesis and low-grade metamorphism has been described by a number of workers (e.g. Ferry 1978, 1979, Veblen & Ferry 1983, White *et al.* 1985, AlDahan & Morad 1986, Morad 1986, 1990, Morad & AlDahan 1986). Ferry (1979) proposed that chlorite replaces biotite through growth of brucite-like layers in the interlayer planes of mica. Veblen & Ferry (1983) studied the mechanism of the biotite–chlorite reaction using high-resolution TEM, and concluded that chlorite forms from biotite by the removal of a tetrahedral sheet from the biotite TOT (tetrahedral–octahedral–tetrahedral) layer and the formation of a brucite-like layer in the chlorite structure. In both mechanisms, the alteration of biotite to chlorite is a layer-by-layer transformation. Replacement of biotite by chlorite through progressive alteration of biotite layers into chlorite layers has been demonstrated by TEM observations in many cases (e.g. Banos *et al.* 1983, Veblen & Ferry 1983, Jiang 1993). It is a reaction that is promoted by both the chemical and structural similarities (trioctahedral 2:1 layers) between biotite and chlorite, and gives rise to coherent layer sequences that directly replace original biotite layers. Such a process would be expected to give rise to optically continuous coherent aggregates, and indeed optical continuity of different chlorite packets within a single grain of a large proportion of undeformed stacks is generally the case.

In contrast to chlorite, discrete mica packets within chlorite–mica stacks do not behave as an optically continuous body. The packets of white mica within chlorite in stacks have lenticular shapes, and they appear to fill cleavage openings in chlorite as observed in SEM images. Layers of white mica are observed to terminate against continuous layers of chlorite at their subparallel boundaries in some TEM lattice fringe images. Such observations are inconsistent with a layer-by-layer alteration mechanism, which requires optical continuity and parallel boundaries between different packets of the same phase within the same grain. Consistent with this relation, no layer-by-layer transformation of biotite to muscovite or phengite has hitherto been documented by TEM observations, although biotite alteration has received intensive investigation (see references above).

Morad & AlDahan (1986) studied the diagenetic alteration of detrital biotite to chlorite and illite, and found that illite appeared to grow along the cleavage planes of biotite rather than to form through layer-by-layer transitions (see fig. 5b in Morad & AlDahan 1986). The chemical dissimilarity between source trioctahedral biotite and product dioctahedral white mica mediates against such direct replacement, and the observations of Morad & AlDahan (1986) are consistent with formation of white mica in stacks during initial deformation of chlorite (+ altered biotite) when strain caused cleavage openings along (001) planes.

Biotite has also been shown to be replaced by expandable, trioctahedral phyllosilicates, which may subsequently be directly replaced by chlorite in prograde sequences. For example, Kisch (1983), Curtis *et al.* (1985), Eggleton & Banfield (1985) and Ilton & Veblen (1988) have demonstrated vermiculite, smectite or hydrobiotite replacements of biotite; the latter studies

showing HRTEM images of direct layer replacements. Jiang (1993) showed in a prograde sequence of pelitic rocks in which both corrensite and chlorite initially replaced biotite of a volcanic origin, and where the expandable component was replaced by chlorite during progressive prograde metamorphism. The general prograde sequence of trioctahedral phyllosilicates transforming from smectite to corrensite to chlorite has been well characterized (e.g. Inoue *et al.* 1984, Inoue & Utada 1991, Shau *et al.* 1990, Shau & Peacor 1989, 1992, Schiffman & Fridleifsson 1991). Initially therefore, biotite may have been altered to vermiculite or trioctahedral smectite and through corrensite to chlorite during the formation of the stacks. Such a sequence is more likely where stacks developed by replacement of amphibole or pyroxene.

The alteration of ferromagnesian minerals, including biotite, to expandable trioctahedral phyllosilicates is one of the earliest water–rock hydration reactions to occur following the eruption of volcanic rocks (e.g. April & Keller 1992). For this reason it is likely that much of the precursor materials for stack development was already partially altered to expandable trioctahedral phyllosilicates prior to turbiditic transport and deposition. The early hydration and vermicular expansion of biotite could explain how these mineral flakes were apparently able to achieve hydrodynamic equivalence with other detritus in the turbidites.

Interaction between chlorite–mica stacks and other phyllosilicates

The BSE images of chlorite–mica stacks show various strain features such as kinking, folding and cross-cutting by cleavage, low-angle boundaries between chorite–mica packets, and an anastomosing network of chlorite and mica. It was therefore fully expected that numerous intracrystalline strain features would be observed at the TEM level. However, TEM study showed little evidence of such strain features. For example, only limited kinking, curvature and numbers of edge dislocations within phyllosilicate packets in stacks are observed in lattice fringe images. Moreover, some boundaries between chlorite and mica packets are apparently semi-coherent to coherent, indicating that there must have been some dissolution–recrystallization along the boundaries with some loss of original textural features. The absence of strain features at the TEM level indicates that phyllosilicates in stacks have been subject to dissolution and crystallization, and that imperfections in crystals associated with strain have been mostly removed. A crystal with a high density of dislocations, such as a plastically deformed crystal, has a greatly increased free energy (internal strain energy). Such crystals tend to recrystallize more readily than crystals with low dislocation densities. For instance, Lee *et al.* (1985) have documented the general decrease in dislocation density of phyllosilicates in shales and slates with increasing degree of diagenesis and metamorphism. This represents a trend toward more perfect, homogeneous crystals with lower internal energy that approaches equilibrium states. These processes are thermally activated and diffusive in nature. Such changes, however, occur very slowly in phyllosilicates at low temperature in the absence of a fluid. The presence of fluid-mediated dissolution and crystallization is demonstrated by the occurrence of chlorite and white mica in the cleavage orientation with subhedral crystal shapes and perfect internal structure. Such crystals have even larger grain sizes than, for example, those euhedral or subhedral chlorite and illite crystals observed in samples from the Salton Sea area, where phyllosilicate have undergone hydrothermal crystallization (Yau *et al.* 1987b) or those in samples from Triassic volcanogenic sediments in Southland, New Zealand, which were formed through crystallization following dissolution of smectite (Ahn *et al.* 1988).

As described in previous sections, white mica and chlorite in stacks have distinctly different compositions from white mica and chlorite in the matrix, suggesting that they formed at different times from different precursor minerals at low temperature. Moreover, bedding- and cleavage-parallel phyllosilicates in the matrix not only have different structural and textural features but also have different compositions, implying formation at different stages. During deformation and cleavage formation, the temperature was relatively high (3*T* micas in the cleavage fabric), diffusion distances were greater, so that Fe, in particular, was supplied from the stacks, and the domains approaching equilibrium were larger than those of bedding-parallel phyllosilicates. Such an explanation is also suggested by the association of discrete phengitic muscovite and paragonite developed in cleavage orientation compared with the occurrence of intermediate Na/K mica in bedding orientation. The occurrence of evolved white mica in bedding-parallel and cleavage-parallel orientations can be related to patterns of regional metamorphism in the central Welsh Basin (Roberts *et al.* 1991, Merriman *et al.* 1992). Crystallization of bedding-parallel white mica is related to a depth-of-burial-related pattern of metamorphism, with grade ranging from late diagenetic to epizonal. Accelerated growth of cleavage-parallel white mica occurred within high strain zones, and generally increased crystallite sizes beyond those generated by burial alone (Roberts *et al.* 1991). A recent study of Sm–Nd dating of clay separates from a prograde sequence of Ordovician pelites in Wales by Ohr *et al.* (1992) showed that uncleaved mudrocks, in which diagenetic bedding-parallel white mica is dominant, give Sm–Nd ages of 458–473 Ma, an age corresponding to the deposition or early burial of sediments. By contrast, the anchizonal and epizonal samples with a well-developed cleavage give Sm–Nd ages as young as 415 Ma but with a large range, which is consistent with the formation of a second population of white mica in response to Lower Devonian regional metamorphism and deformation at *ca* 390 Ma. These results further verify that mudrocks in the Welsh basin have undergone dissolution–crystallization during low-grade metamorphism.

Dissolution–crystallization can give rise to discontinuous changes in the composition of white mica and chlorite (Knipe 1979, Lee & Peacor 1985). When K and Al are available in solution, illite exhibits an increase in both K and Al and a decrease in Si as it approaches the ideal muscovite composition (e.g. Hower *et al.* 1976, Hoffman & Hower 1979). In this case, however, no significant increase in K and Al components was found in white mica parallel to the cleavage compared to white mica parallel to bedding, simply because the latter had already attained a composition approaching that of evolved mica. On the other hand, the ranges in Na component of cleavage-parallel and bedding-parallel white mica are different. High Na/(Na+K) ratios characterize the bedding-parallel white mica and reflect an unusually high Na content in the original turbidite mud matrix. This implies that the original matrix was smectite-rich and probably derived from argillized glassy ash rich in Na and other exchangeable cations. Cleavage-parallel white mica has compositions intermediate between those of bedding-parallel white mica and white mica in chlorite–mica stacks. It is similar to the former in its higher Na/(Na+K) ratios and to the latter in its higher Si/Al and Fe/(Fe+Mg) ratios, and Fe and Mg contents. The phengitic component of white mica in the cleavage orientation is representative of higher grade conditions, and consistent with the occurrence of 3*T* polytype. Moreover, cleavage-parallel chlorite also has a Fe composition intermediate to that parallel to bedding (lower Fe content) and that in stacks (higher Fe content). In contrast, Knipe (1979) observed that the Fe content of chlorite in the bedding orientation is relatively greater than that of cleavage-parallel chlorite. Similar observations have also been made in shaly limestone of the Kalkburg Formation, New York, where chlorite that was formed during pressure solution tends to have lower Fe contents (Kreutzberger & Peacor 1988). The relatively higher Fe content of cleavage-parallel chlorite compared to that of chlorite in the bedding orientation in this study is probably due to partial dissolution of chlorite in the stacks. This is consistent with the interpretation that chlorite–mica stacks are actively involved in the chemical changes that occur during cleavage formation (see also Beach 1979). Partial dissolution of both stacks and bedding-parallel phases provided the constituents that resulted in the compositions of the cleavage-parallel white mica and chlorite being different from those of their bedding-parallel equivalents. Thus, the changes in composition of white mica and chlorite are related to the components available in solution and in pre-existing minerals, i.e. pre-existing chlorite–mica stacks also contributed to the formation of cleavage-parallel phyllosilicates in slates in central Wales.

In summary, the textural and mineralogical evolution of chlorite–mica stacks and phyllosilicates in the matrix can be described as follows.

Stage 1. Deposition of turbiditic mud consisting of volcanogenic biotite, amphibole and pyroxene, together with other detrital grains, in a smectite-rich matrix; all three ferromagnesian minerals may already have been partially altered to expandable trioctahedral phyllosilicates at this stage.

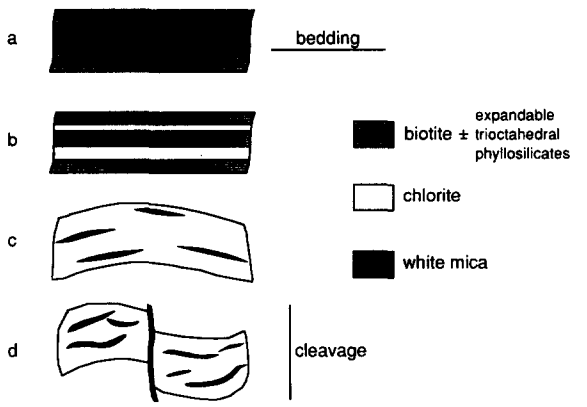

Fig. 12. Schematic evolution of a biotite grain to chlorite–mica stacks during alteration and cleavage development. An initial biotite grain (a) is altered to chlorite via layer-to-layer transition (b). Chlorite–mica stacks develop by formation of mica filling the cleavage openings in chlorite during deformation, accompanied by shortening parallel to basal planes (c). Cleavage formation results in continued shortening, deformation of chlorite–mica stacks, and a new orientation of white mica (d).

Stage 2. Early diagenetic alteration of relict biotite and other trioctahedral phyllosilicates, to chlorite via layer-by-layer transformation (perhaps with an intermediate expandable component) (Figs. 12a & b); transformation of smectite clay to illite–smectite and chlorite–smectite mixed-layer minerals.

Stage 3. Progressive burial leading to white mica filling of 001 fissures of chlorite (Fig. 12c) as a chlorite–mica stacks developed during late diagenesis and very low-grade burial metamorphism; matrix phyllosilicates were transformed to white mica (2*M* polytype) and chlorite, and a bedding-parallel fabric was enhanced in the mudstone.

Stage 4. Lower Devonian deformation and metamorphism resulted in modification of stacks during cleavage development in the mudstone; fissures formed in the stacks were filled by white mica (Fig. 12d); cleavage-parallel chlorite and white mica formed by dissolution-crystallization of bedding-parallel phyllosilicates; intracrystalline defects in chlorite within stacks were annealed by migration of defects and by dissolution–crystallization with diffusion of Fe from stacks to cleavage-parallel chlorite; late white mica formed in cross-cutting seams in deformed stacks.

Acknowledgements—We thank Y.-H. Shau, W.-T. Jiang and C. Henderson for their help with instruments at the University of Michigan Electron Microbeam Analysis Laboratory. We are grateful to Dr R. J. Lisle and an anonymous reviewer for their critical reviews. This work is supported by NSF grants EAR-88-17080 and EAR-91-04565 to D. R. Peacor. The analytical STEM used in this study was acquired under grant No. EAR-87-08276, the SEM under grant No. BSR-83-14092, and the microprobe under grant No. EAR-82-12764 from the National Science Foundation. R. J. Merriman publishes by permission of the Director, British Geological Survey (N.E.R.C.).

REFERENCES

Aguirre, L. & Atherton, M. P. 1987. Low-grade metamorphism and

geotectonic setting of Macuchi Formation, western Cordilera of Ecuador. *J. metamorph. Geol.* **5**, 473–494.

Ahn, J. H., Peacor, D. R. & Essene, E. J. 1985. Coexisting paragonite–phengite in blueschist eclogite: a TEM study. *Am. Miner.* **70**, 1193–1204.

Ahn, J. H. & Peacor, D. R. 1986. Transmission and analytical electron microscopy of the smectite-to-illite transition. *Clays Clay Miner.* **34**, 165–179.

Ahn, J. H., Peacor, D. R. & Coombs, D. S. 1988. Formation mechanisms of illite, chlorite and mixed layer illite–chlorite in Triassic volcanogenic sediments from the Southland Syncline, New Zealand. *Contr. Miner. Petrol.* **99**, 82–89.

AlDahan, A. A. & Morad, S. 1986. Chemistry of detrital biotites and their phyllosilicate intergrowths in sandstones. *Clays Clay Miner.* **34**, 539–548.

April, R. H. & Keller, D. M. 1992. Saponite and vermiculite in amygdales of the Granby basaltic tuff, Connecticut Valley. *Clays Clay Miner.* **40**, 22–31.

Attlewell, P. B. & Taylor, R. K. 1969. A microtextural interpretation of a Welsh slate. *Int. J. Rock Mech. & Mining Sci.* **6**, 423–428.

Awan, M. A. & Woodcock, N. H. 1991. A white mica crystallinity study of the Berwyn Hills, North Wales. *J. metamorph. Geol.* **9**, 765–773.

Banos, J. O., Amouric, M., Fouquet, C. & Baronnet, A. 1983. Interlayering and Interlayer slip in biotite as seen by HRTEM. *Am. Miner.* **68**, 754–758.

Bayliss, S. W. 1975. Nomenclature of the trioctahedral chlorites. *Can. Mineral.* **13**, 178–180.

Bayly, B. M., Borradaile, G. J. & Powell, C. McA. 1977. *Atlas of Rock Cleavage*. University of Tasmania Press, Hobart.

Beach, A. 1979. Pressure solution as a metamorphic process in deformed terrigeneous sedimentary rocks. *Lithos* **12**, 51–58.

Beutner, E. C. 1978. Slaty cleavage and related strain in Martinsburg slate, Dalaware Water Gap, New Jersey. *Am. J. Sci.* **278**, 1–23.

Blencoe, J. G. & Luth, W. C. 1973. Muscovite-paragonite solvi at 2.4 and 8 kb pressure. *Geol. Soc. Am. Abs. W. Prog.* **5**, 553–554.

Boles, J. R. & Coombs, D. S. 1977. Zeolite facies alteration of sandstones in the Southland syncline, New Zealand. *Am. J. Sci.* **277**, 982–1012.

Brenchley, P. J. 1969. Origin of matrix in Ordovician greywackes, Berwyn Hills, North Wales. *J. sedim. Petrol.* **39**, 1297–1301.

British Geological Survey 1992. Rhayader. England & Wales Sheet 179. Solid. 1:50,000. Ordnance Survey for British Geological Survey, Southampton.

Buseck, P. R. & Cowley, J. M. 1983. Modulated and intergrowth structures in minerals and electron microscope methods for their study. *Am. Miner.* **68**, 18–40.

Craig, J., Fitches, W. R. & Maltman, A. J. 1982. Chlorite–mica stacks in low strain rocks from central Wales. *Geol. Mag.* **119**, 243–256.

Curtis, C. D., Hughes, C. R., Whiteman, J. A. & Whittle, C. K. 1985. Composition variation within some sedimentary chlorite and some comments on their origin. *Mineralog. Mag.* **49**, 375–386.

Dimberline, A. J. 1986. Electron microscope and electron microprobe analysis of chlorite–mica stacks in the Wenlock turbidites, mid Wales, U.K. *Geol. Mag.* **123**, 299–306.

Eggleton, R. A. & Banfield, J. F. 1985. The alteration of granitic biotite to chlorite. *Am. Miner.* **70**, 902–910.

Eugster, H. P. 1956. Muscovite-paragonite join and its use as a geological thermometer. *Bull. geol. Soc. Am.* **67**, 1693.

Eugster, H. P., Albee, A. L., Beace, A. E., Thompson, J. B., Jr & Waldbuam, D. R. 1972. The two phase region and excess mixing properties of paragonite-muscovite crystalline solutions. *J. Petrol.* **13**, 147–179.

Evans, L. J. & Adams, W. A. 1975. Chlorite and illite in some lower Paleozoic mudstones of mid Wales. *Clay Miner.* **10**, 387–397.

Evarts, R. C. & Schiffman, P. 1983. Submarine hydrothermal metamorphism of the Del Puerto ophiolite, California. *Am. J. Sci.* **283**, 289–340.

Ferry, J. M. 1978. Fluid interaction between granite and sediment during metamorphism, south-central Maine. *Am. J. Sci.* **278**, 1025–1056.

Ferry, J. M. 1979. Reaction mechanisms, physical conditions, and mass transfer during hydrothermal alteration of mica and feldspar in granitic rocks from south-central Maine, U.S.A. *Cont. Miner. Petrol.* **68**, 125–139.

Fitches, W. K. & Johnson, R. 1978. Cleavage–fold relationships in the Aberystwyth Grits: A preliminary report. In: *Deformation of Soft Sediments* (edited by Fitches, W. R. & Maltman, A. J.). *J. geol. Soc. Lond.* **135**, 245–251.

Fletcher, C. J. N., Davis, J. R., Waters, R. A., Wilson, D. & Zalasiewicz, J. A. In press. Geology of the country between Llanilar and Rhayader. Explanation for 1:50,000 Sheets 178 and 179 (England & Wales). HMSO for British Geological Survey, London.

Frey, M. 1970. The steps from diagenesis to metamorphism in pelitic rocks during Alpine orogenies. *Sedimentology* **15**, 261–279.

Frey, M. 1978. Progressive low-grade metamorphism of a black shale formation, central Swiss Alps, with special reference to pyrophyllite and margarite bearing assemblages. *J. Petrol.* **19**, 95–135.

Hayes, J. B. 1970. Polytypism of chlorite in sedimentary rocks. *Clays Clay Miner.* **18**, 285–306.

Hoeppener, R. 1956. Zum Problem der Bruchbildung Schieferung und Faltung. *Geol. Rdsch.* **45**, 247–283.

Hoffman, J. & Hower, J. 1979. Clay mineral assemblages as low-grade metamorphic geothermometers: application to thrust faulted disturbed belt of Montana, U.S.A. In: *Aspects of Diagenesis* (edited by Scholle, P. A. & Schluger, P. R.). *Spec. Publs. Soc. econ. Paleont. Mineral.* **26**, 55–59.

Holeywell, R. C. & Tullis, T. E. 1975. Mineral reorientation and slaty cleavage in the Martinsburg formation, Lehigh Gap, Pennsylvania. *Bull. geol. Soc. Am.* **86**, 1296–1304.

Howells, M. F., Reedman, A. J. & Campbell, S. D. G. 1991. Ordovician (Caradoc) marginal basin volcanism in Snowdonia (north-west Wales). HMSO for British Geological Survey, London.

Hower, J., Eslinger, E. V., Hower, M. E. & Perry, E. A. 1976. Mechanism of burial metamorphism of argillaceous sediments: 1. Mineralogical and chemical evidence. *Bull geol. Soc. Am.* **87**, 725–737.

Huff, W. D. & Morgan, D. G. 1989. Stratigraphy, mineralogy and tectonic setting of Silurian K-bentonites in southern England and Wales. In: *Proceedings of the 9th International Clay Conference* (edited by Farmer, V. C. & Tardy, Y.). *Mem. Geol. Soc.* **8**, 33–42.

Ilton, E. S. & Veblen, R. D. 1988. Copper inclusions in sheet silicate from porphyry Cu deposits. *Nature* **334**, 516–518.

Inoue, A., Utada, M., Negata, H. & Waltanabe, T. 1984. Conversion of trioctahedral smectite to interstratified chlorite/smectite in Pliocene acidic pryoclastic sediments of the Ohyu district, Arita Prefecture, Japan. *Clay Sci. Soc. Japan* **6**, 103–116.

Inoue, A. & Utada, M. 1991. Smectite-to-chlorite transformation in thermal metamorphism of volcanoclastic rocks at Kamikita area, northern Honshu, Japan. *Am. Miner.* **76**, 628–640.

Jiang, W.-T. 1993. Diagenesis and very low-grade metamorphism of pelitic rocks from the Gaspé Peninsula Québec. Unpublished. Ph.D. thesis, University of Michigan, Ann Arbor, Michigan.

Kisch, H. J. 1983. Mineralogy and petrology of burial diagenesis (burial metamorphism) and incipient metamorphism in clastic rocks. In: *Diagenesis in Sediments and Sedimentary Rocks* (edited by Larsen, G. & Chilingar, G.V.). Elsevier, New York, 289–493.

Knipe, R. J. 1979. Chemical changes during slaty cleavage development. *Bull. Mineral.* **102**, 206–209.

Kossovskaya, A. G. & Shutov, V. D. 1970. Main aspects of epigenesis problem. *Sedimentology* **15**, 11–40.

Kreutzberger, M. E. & Peacor, D. R. 1988. Behavior of illite and chlorite during pressure solution of shaly limestone of the Kalkberger Formation, Catskill, New York. *J. Struct. Geol.* **10**, 803–811.

Kubler, B. 1968. Evaluation quantitative du metamorphisme par la cristallinite de L'illite. *Bull. Centre Rech. Pau. SNPA* **2**, 385–397.

Lee, J. H., Ahn, J. H. & Peacor, D. R. 1985. Textures in layered silicates: progressive changes through diagenesis and low-temperature metamorphism. *J. sedim. Petrol.* **55**, 532–540.

Lee, J. H. & Peacor, D. R. 1985. Ordered 1:1 interstratification of illite and chlorite: A transmission and analytical electron microscopy study. *Clays Clay Miner.* **33**, 463–467.

Lee, J. H., Peacor, D. R., Lewis, D. D. & Wintsch, R. P. 1984. Chlorite–illite/muscovite interlayered and interstratified crystals: A TEM/STEM study. *Contr. Miner. Petrol.* **88**, 372–385.

Lee, J. H., Peacor, D. R., Lewis, D. D. & Wintsch, R. P. 1986. Evidence for syntectonic crystallization for the mudstone to slate transition at Lehigh Gap, Pennsylvania, U.S.A. *J. Struct. Geol.* **8**, 767–780.

Li, G., Peacor, D. R., Merriman, R. J. & Roberts, B. 1992. TEM and AEM study of chlorite–mica stacks in slates, central Wales, U.K. *29th Int. Geol. Congr. Kyoto, Japan Abs.* **1**, 100.

Li, G., Peacor, D. R., Merriman, R. J. & Roberts, B. In revision. The diagenetic to low-grade metamorphic evolution of matrix white micas in the system muscovite-paragonite in a mudrock from Central Wales, UK. *Clays Clay Miner.*

Merriman, R. J., Roberts, B. & Hirons, S. R. 1992. Regional low grade metamorphism in the central part of the Lower Palaeozoic Welsh Basin: an account of the Llanilar and Rhayader districts,

BGS 1:50 k sheets 178 and 179. British Geological Survey Technical Report WG/92/16.

Merriman, R. J., Roberts, B. & Peacor, D. R. 1990. A transmission electron microscope study of white mica crystallite size distribution in a mudstone to slate transitional sequence, North Wales, U.K. *Contr. Miner. Petrol.* **106**, 27–40.

Milodowski, A. E. & Zalasiewicz, J. A. 1991. The origin and sedimentary, diagenetic and metamorphic evolution of chlorite–mica stacks in Llandovery sediments of central Wales, U.K. *Geol. Mag.* **128**, 263–278.

Morad, S. 1986. Mica–chlorite intergrowths in very low-grade metamorphic sedimentary rocks from Norway. *Neues Jb. Mineral, Abh.* **154**, 271–287.

Morad, S. 1990. Mica alteration reactions in Jurassic reservoir sandstones from the Haltenbanken area, offshore Norway. *Clays Clay Miner.* **38**, 584–590.

Morad, S. & AlDahan 1986. Diagenetic alteration of detrital biotite in Proterozoic sedimentary rocks from Sweden. *Sediment. Geol.* **47**, 95–107.

Ohr, M., Li, G., Peacor, D. R. & Halliday, A. N. 1992. Sm–Nd dating of diagenetic vs tectonic events in a prograde sequence of pelites, Wales, U.K. *V. M. Goldschmidt Conf. Abs.* **1992**.

Pharaoh, T. C., Merriman, R. J., Evans, J. A., Brewer, T. S., Webb, P. C. & Smith, N. P. J. 1991. Early Paleozoic arc-related volcanism in the concealed Caledonides of southern Britain. *Anns. Soc. géol. Belg.* **114**, 63–91.

Pye, K. & Krinsley, D. H. 1983. Inter-layered clay stacks in Jurassic shales. *Nature* **304**, 618–620.

Ramamohana Rao, T. 1977. Distribution of elements between coexisting phengite and chlorite from the greenschist facies of the Tennant Creek area, central Australia. *Lithos* **10**, 103–112.

Roberts, B. & Merriman, R. J. 1990. Cambrian and Ordovician metabentonites and their relevance to the origins of associated mudrocks in the northern sector of the Lower Palaeozoic Welsh marginal basin. *Geol. Mag.* **127**, 31–43.

Roberts, B., Merriman, R. J. & Pratt, W. 1991. The influence of strain, lithology and stratigraphical depth on white mica (illite) crystallinity in mudrocks from the vicinity of the Corris Slate Belt, Wales: implications for the timing of metamorphism in the Welsh Basin. *Geol. Mag.* **128**, 633–645.

Robinson, D. & Bevins, R. E. 1986. Incipient metamorphism of the Lower Palaeozoic marginal basin of Wales. *J. metamorph. Geol.* **4**, 101–113.

Roy, A. B. 1978. Evolution of slaty cleavage in relation to diagenesis and metamorphism: a study from the Hunsruckschiefer. *Bull. geol. Soc. Am.* **89**, 1775–1785.

Schiffman, P. & Fridleifsson, G. O. 1991. The smectite to chlorite transition in Drillhole NJ-15, Nesjavellir Geothermal Field, Iceland: XRD, BSE and electron microprobe investigations. *J. metamorph. Geol.* **9**, 679–696.

Shau, Y.-H. & Peacor, D. R. 1989. Phyllosilicates in hydrothermally altered basalts from DSDP Hole 504B, Leg 83—a TEM and AEM study (Abstr). *Geol. Soc. Am. Abs. w. Prog.* **21**, A119.

Shau, Y.-H. & Peacor, D. R. 1992. Phyllosilicates in hydrothermally altered basalts from DSDP Hole 504B, Leg 83—a TEM and AEM study. *Cont. Miner. Petrol.* **112**, 119–133.

Shau, Y.-H., Peacor, D. R. & Essene, E. J. 1990. Corrensite and mixed-layer chlorite/corrensite in metabasalt from northern Taiwan: TEM/AEM, EMPA, XRD, and optical studies. *Contr. Miner. Petrol.* **105**, 123–142.

Środoń, J., Morgan, D. J., Eslinger, E. V., Eberl, D. D. & Karlinger, M. R. 1986. Chemistry of illite/smectite and end-member illite. *Clays Clay Miner.* **34**, 368–378.

Teale, C. T. & Spears, D. A. 1986. The mineralogy and origin of some Silurian bentonites, Welsh Borderland, U.K. *Sedimentology* **33**, 757–765.

van der Pluijm, B. A. & Kaars-Sijpesteijn, C. H. 1984. Chlorite–mica aggregates; morphology, orientation, development and bearing on cleavage formation in very low-grade rocks. *J. Struct. Geol.* **6**, 399–407.

Veblen, D. R. & Ferry, J. M. 1983. A TEM study of the biotite–chlorite reaction and comparison with petrographical observation. *Am. Miner.* **68**, 1160–1168.

Voll, G. 1960. New work on petrofabrics. *Liverpool Manchester Geol. J.* **2**, 503–597.

Weaver, Ch. E. R. 1984. Shale–slate metamorphism in southern Appalachian. In: *Development in Petrology, Vol.* 10. Elsevier, Amsterdam.

Weber, K. 1981. Kinemetic and metamorphic aspects of cleavage formation in very low grade metamorphic slates. *Tectonophysics* **78**, 297–306.

White, S. H., Huggett, J. M. & Shaw, H. F. 1985. Electron-optical studies of phyllosilicate intergrowths in sedimentary and metamorphic rocks. *Mineralog. Mag.* **49**, 413–423.

White, S. H. & Knipe, R. J. 1978. Microstructure and cleavage development in selected slates. *Contr. Miner. Petrol.* **66**, 165–174.

Williams, P. F. 1972. Development of metamorphic layering and cleavage in low grade metamorphic rocks at Bermagni, Australia. *Am. J. Sci.* **272**, 1–47.

Woodland, B. G. 1982. Gradational development of dominant slaty cleavage, its origin and relation to chlorite porphyroblasts on the Martinsburg Formation, eastern Pennsylvania. *Tectonophysics* **82**, 89–124.

Woodland, B. G. 1985. Relationship of concretions and chlorite–muscovite porphyroblasts to the development of domainal cleavage in low-grade metamorphic deformed rocks from north-central Wales, Great Britain. *J. Struct. Geol.* **7**, 205–215.

Yau, Y.-C., Peacor, D. R. & Essene, E. J. 1987a. Hydrothermal treatment of smectite, illite and basalt to 460°C: Comparison of natural with hydrothermally formed clay minerals. *Clays Clay Miner.* **35**, 241–250.

Yau, Y. -C., Peacor, D. R. & McDowell, S. D. 1987b. Smectite to illite reaction in Salton Sea shales: A transmission and analytical electron microscopy study. *J. sedim. Petrol.* **57**, 335–342.